Stanford Exploration Project, Report 112, November 11, 2002, pages 37–47

Dealing with errors in automatic velocity analysis

Robert G. Clapp[1]

ABSTRACT

The lack of human interaction in automatic reflection tomography leads to a larger percentage of "bad" data points. The number of data points associated with events with spurious moveouts (such as multiples and converted waves) can be minimized by intelligently controlling the semblance scanning range. The effect of the bad data points can be limited by replacing the standard L_2 norm solution with a norm closer to L_1 by reweighted least-squares. By replacing the standard constant ϵ parameter with a diagonal operator, areas with large errors in moveout can be highly regularized with minimal effect on areas with more reliable moveout information. This methodology is applied to a complex 2-D dataset.

INTRODUCTION

In ray-based reflection tomography, picking reflectors is an integral and painful part of the process (Clapp, 2001b; van Trier, 1990; Stork, 1992; Kosloff et al., 1996). The common methodology is to pick a series of reflectors from a migrated image. A set of rays are then calculated that reflect at the picked interfaces. A major problem is the human intensive nature of reflector picking, especially for 3-D data. Automatic pickers can help, but significant human quality control (QC) is still necessary. A high level of QCing is required because inaccurate reflector picks lead to inaccurate reflector dip estimates. These poor estimates cause information to be back projected to the wrong portion of the model space, seriously hampering the inversion.

Woodward et al. (1998) and Clapp (2001a) introduced methods to limit the amount of picking required by selecting back projection points based on criteria such as semblance and dip coherence. These methods are successful in reducing the human cost of tomography but have two significant weaknesses. First, moveout is often characterized by a single value. This value is obtained by scanning over a range of moveouts and then selecting the maximum. In areas with significant multiple or converted wave energy, they will often have trouble distinguishing primary reflections (signal) from multiple and converted wave reflections (noise). The second problem is that these automatic point selection methods are generally going to have a larger level of erroneous moveout descriptions that generally increase with depth. These erroneous moveouts will generally cause large residuals which can dominate the inversion procedure.

[1]**email:** bob@sep.stanford.edu

In this paper, I show three simple methods to combat both problems. Unreasonable moveouts can be avoided by scanning over a large range of moveouts but only selecting points whose maximum is in a narrower range of moveouts. Second, I show that we can account for a higher level of variance by adding a diagonal weight to our model styling goal. Finally, I show that the effect of the remaining non-primary events and other erroneous moveouts can be further diminished by using re-weighted least-squares (Claerbout, 1998) to simulate a L_1 inversion problem where noisy data points have less of an effect.

LIMITING THE SCANNING RANGE

In Clapp (2001a), I outlined a procedure for selecting points for back projection. The goal was to find points with high dip coherence and semblance at a minimum distance from each other. This methodology can run into problems for events whose moveout doesn't correspond to primary events or whose moveout is not adequately defined by calculating vertical semblance. For example, the common reflection point (CRP) gathers in Figure 1 shows every fifth gather along the left edge of a salt body. Note the coherent but "hockey stick" like shapes within the 'A' oval. These can be caused by small velocity errors (Biondi and Symes, 2002) but measuring just vertical moveout would indicate much larger errors. Clapp (2002) shows one way to address the latter concern.

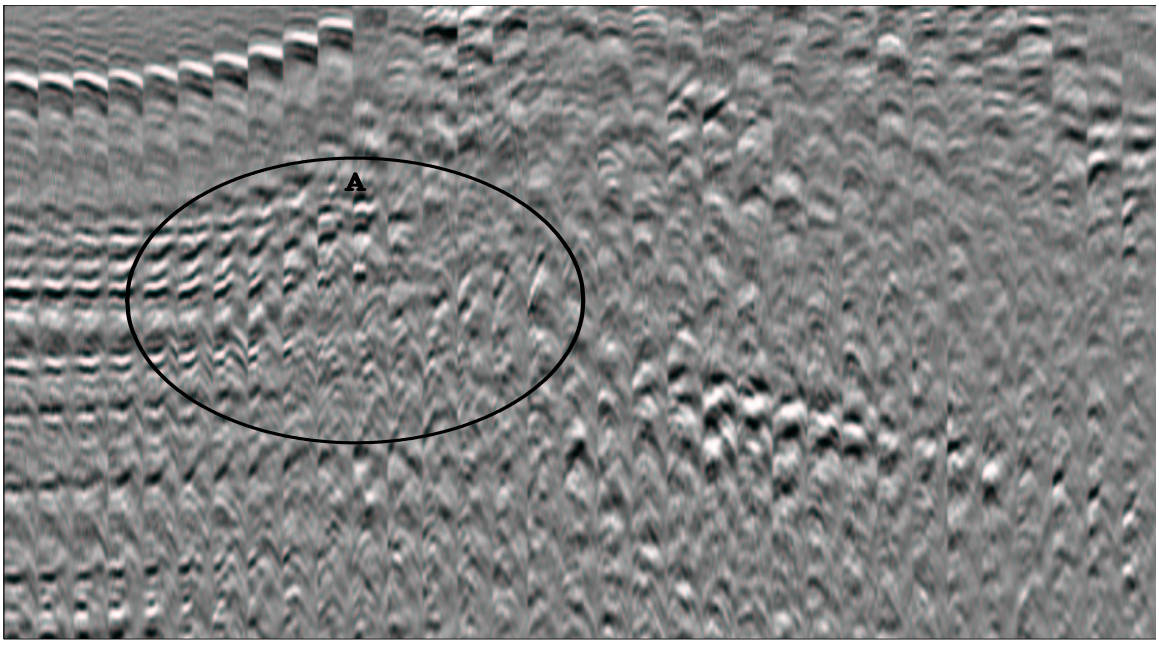

Figure 1: Every 5th gather to the left edge of a salt body. Note the coherent, "hockey stick" behavior within 'A'. bob3-gathers [CR]

Simply limiting the range of acceptable moveouts that we search isn't a sufficient solution because the maximum often will be at the extreme scan range. A simple methodology to minimize the effect of unreasonable moveouts is to scan over a large range of acceptable

moveouts and only accept points whose maximum fall within a smaller range (see Figure 2). With this methodology, spurious moveouts can be identified and ignored. When dealing with internal multiples or events whose moveout is close to acceptable, failure can still result.

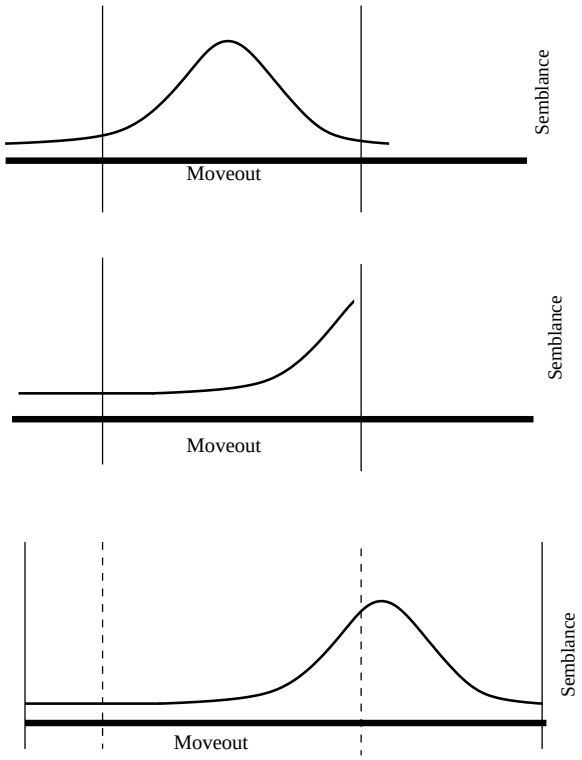

Figure 2: The top figure shows an example of a good point. The maximum is reasonable and within the scanning region indicated by the solid vertical lines. The second plot shows the problematic situation. The moveout is unreasonable and its maximum is outside the scanning range. We can avoid using the unrealistic moveout by scanning over moveouts between the solid lines but only selecting points whose maximum is within the dashed lines, bottom panel. bob3-limited [NR]

To show the benefits of this methodology, I applied it to a complex 2-D dataset. Figure 3 shows an initial velocity model and migrated image of a 2-D line from a 3-D dataset donated by Total Fina Elf. Figure 4 shows the updated velocity model and migrated image without limiting the scan range. Note the extreme velocity along the edge of the salt. The resulting image is less coherent than the initial image, especially in the ovals indicated by ‘A’, ‘B’, and ‘C’. Figure 5 shows the result of limiting the range of acceptable moveouts. Note how the velocity along the edge is more reasonable. We see a strong salt bottom reflection at ‘A’, better definition of the valley at ‘B’, and more coherent events leading up to the salt edge at ‘C’.

VARIABLE EPSILON

Let’s begin with a review of the general fitting goals we are using for the tomography problem.

Tomography Review

Following the methodology of Clapp and Biondi (1999), I will begin by considering a regularized tomography problem. I will linearize around an initial slowness estimate and find a linear operator in the vertical traveltime domain $\mathbf{T}$ between our change in slowness $\Delta\mathbf{s}$ and

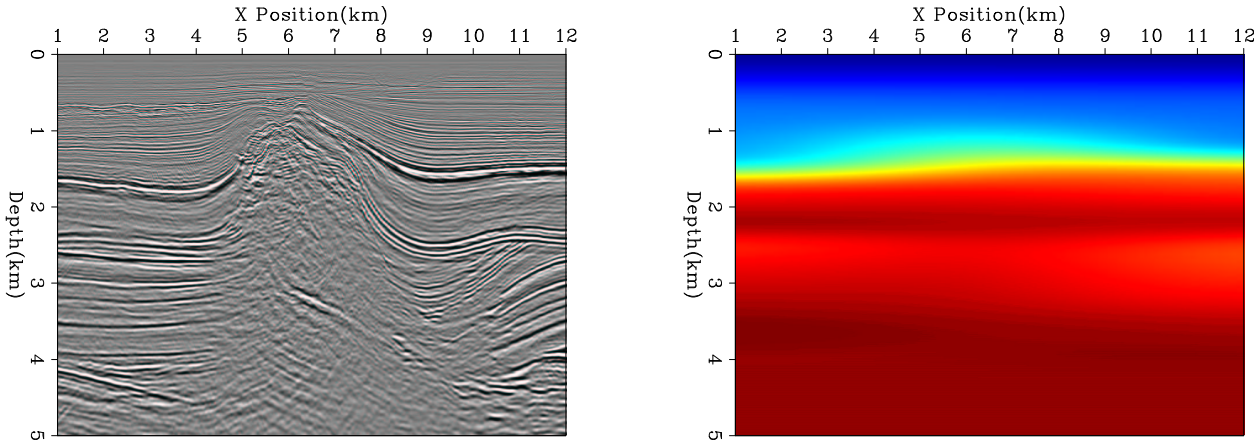

Figure 3: The starting model and migration of a 2-D line from a 3-D North Sea dataset. The top-left panel shows the velocity model (white indicates large velocities) and the top-right panel shows the migrated image using this velocity. The bottom panel shows a zoomed area around the salt body. Note the salt bottom,'A'; the valley structure at 'B'; and over the salt under-hang at 'C'. bob3-combo.vel0 [CR,M]

our change in traveltimes $\Delta\mathbf{t}$. We will write a set of fitting goals,

$$\begin{aligned} \Delta\mathbf{t} &\approx \mathbf{T}\Delta\mathbf{s} \\ \mathbf{0} &\approx \epsilon\mathbf{A}\Delta\mathbf{s}, \end{aligned} \tag{1}$$

where $\mathbf{A}$ is our steering filter operator (Clapp et al., 1997) and ϵ is a Lagrange multiplier. However, these fitting goals don't accurately describe what we really want. Our steering filters are based on our desired slowness rather than change of slowness. With this fact in mind, we can rewrite our second fitting goal as:

$$\begin{aligned} \mathbf{0} &\approx \epsilon\mathbf{A}(\mathbf{s_0}+\Delta\mathbf{s}) \\ -\epsilon\mathbf{A}\mathbf{s_0} &\approx \epsilon\mathbf{A}\Delta\mathbf{s}. \end{aligned} \tag{2}$$

Our second fitting goal can not be strictly defined as regularization but we can still do a preconditioning substitution (Fomel et al., 1997), giving us a new set of fitting goals:

$$\begin{aligned} \Delta\mathbf{t} &\approx \mathbf{T}\mathbf{A}^{-1}\mathbf{p} \\ -\epsilon\mathbf{A}\mathbf{s_0} &\approx \epsilon\mathbf{I}\mathbf{p}. \end{aligned} \tag{3}$$

Our standard inversion fitting goals (3) make an assumption that our data fitting goal is equally believable everywhere. Stated another way, we want the same weight ϵ for our model styling goal everywhere. This is generally untrue. We can, and should, account for differing level of confidence in two different ways. If we have a measure of certainty about a data point (for example how much of a peak our semblance pick is) we can add a data covariance operator $\mathbf{W}$ to our fitting goals,

$$\begin{aligned} \mathbf{W}\Delta\mathbf{t} &\approx \mathbf{W}\mathbf{T}\mathbf{A}^{-1}\mathbf{p} \\ -\mathbf{A}\mathbf{s_0} &\approx \epsilon\mathbf{I}\mathbf{p}. \end{aligned} \tag{4}$$

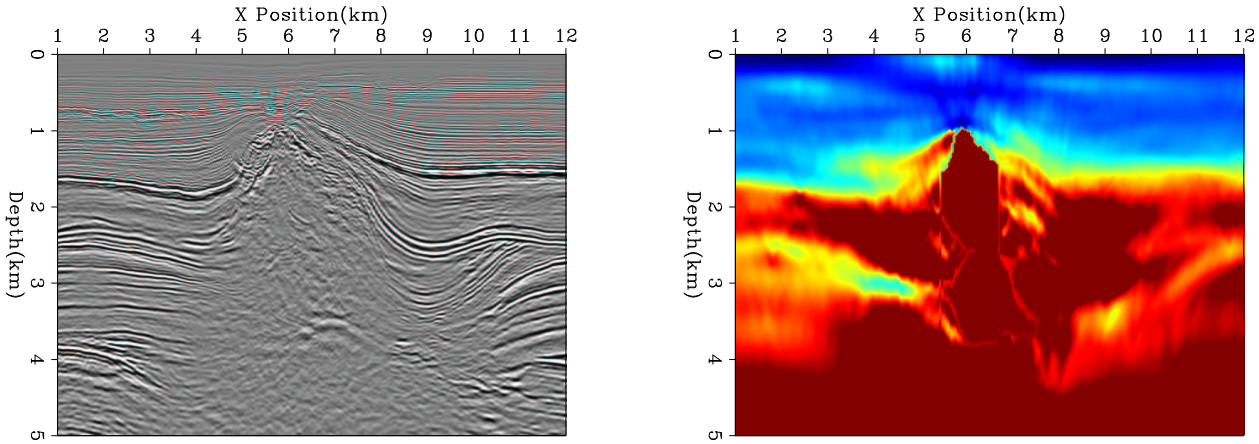

Figure 4: Data after one non-linear iteration. The top-left panel shows the velocity model and the top-right panel shows the migrated image using this velocity. The bottom panel shows a zoomed area around the salt body. Note the salt bottom,'A'; the valley structure at 'B'; and under the salt over-hang at 'C'. bob3-combo.vel1.bad [CR,M]

We can also often make statements about our confidence in our data fitting goal as a function of our model space. For example, generally as we get deeper, we will have less confidence in the points, and be less able to get a high frequency velocity model. We can account for this uncertainty by replacing the constant epsilon of fitting goal (4) with a diagonal weighting operator **E** resulting in the updated fitting goals,

$$\begin{aligned} \mathbf{W}\Delta\mathbf{t} &\approx \mathbf{W}\mathbf{T}\mathbf{A}^{-1}\mathbf{p} \\ -\mathbf{E}\mathbf{A}\mathbf{s_0} &\approx \mathbf{E}\mathbf{I}\mathbf{p}. \end{aligned} \tag{5}$$

By having this additional freedom we can allow for more model variability in the near surface and force more smoothing at deeper locations. Figure 6 shows the result of using the new fitting goals (5). Note how we have a higher frequency velocity structure above and a smoother below. The overall image quality is also improved compared to Figure 5.

L_1 NORM TO HANDLE LARGE RESIDUALS

The previous section discussed a method to reduce the number of bad data points. Another approach is to limit their effect in the inversion. Generally we do not iterate to convergence. Early iterations tend to concentrate on large residuals. Erroneous data points tend to cause the large residuals. The result is that our solutions tend to be dominated by these erroneous data points.

A method to combat this problem is to change our misfit functional from the traditional

$$\mathbf{r_d} = \|\mathbf{d} - \mathbf{L}\mathbf{m}\|^2. \tag{6}$$

There are two different methods to change the misfit function. The first is to use a non-linear solver. With a non-linear solver there are a variety of misfit functions, most interestingly the

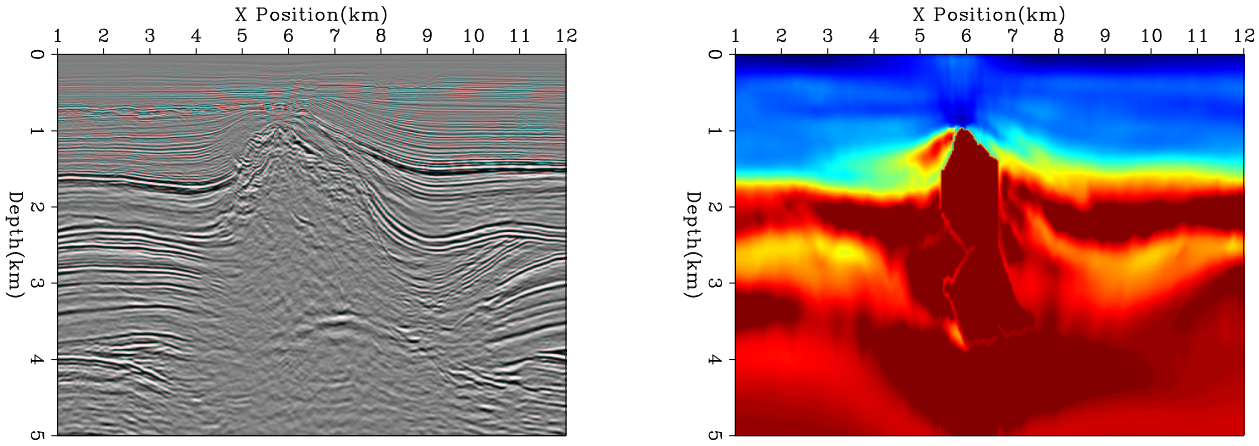

Figure 5: Data after one non-linear iteration with limited semblance search window. The top-left panel shows the velocity model and the top-right panel shows the migrated image using this velocity. The bottom panel shows a zoomed area around the salt body. Note the salt bottom,'A'; the valley structure at 'B'; and under the salt over-hang at 'C'. Note the improvements compared to Figure 4. bob3-combo.vel1.l2 [CR,M]

Ł$_1$ and Huber functionals (Huber, 1973; Claerbout, 1996; Clapp and Brown, 1999). A second approach is reweighted least-squares, (Nichols, 1994; Guitton, 2000). In reweighted least-squares a weighting operator is applied to the residuals based upon the size of residuals at certain points in the inversion.

The total non-linear approach has fewer parameters to manipulate and is generally more robust than reweighted approach. The downside of the completely non-linear approach is that it is significantly slower (a factor of ten or more is not uncommon). I chose the reweighted least-squares approach because I am most interested in finding and minimizing the effect of the largest residuals. I found that a single calculation of the weighting function after $\frac{1}{3}$ of the total number of iterations was sufficient to minimize the most troublesome residuals. Figure 7 shows the velocity and migration result using an L_1 norm. Note the improvement in image quality over either of the previous approaches (Figures 4 and 5). The salt bottom is more continuous, 'A'. The valley structure is better defined, 'B'. The reflectors are more continuous and extend closer to the salt at 'C'.

CONCLUSIONS

Automatic velocity updating has great potential for reducing processing cycle time. The problem of automatic methods selecting unreasonable moveouts can be reduced by scanning over a large moveout range and selecting events which fall within a smaller window. The effect of bad points can be further reduced by replacing the standard L_2 norm with a L_1 norm. Preliminary results are promising.

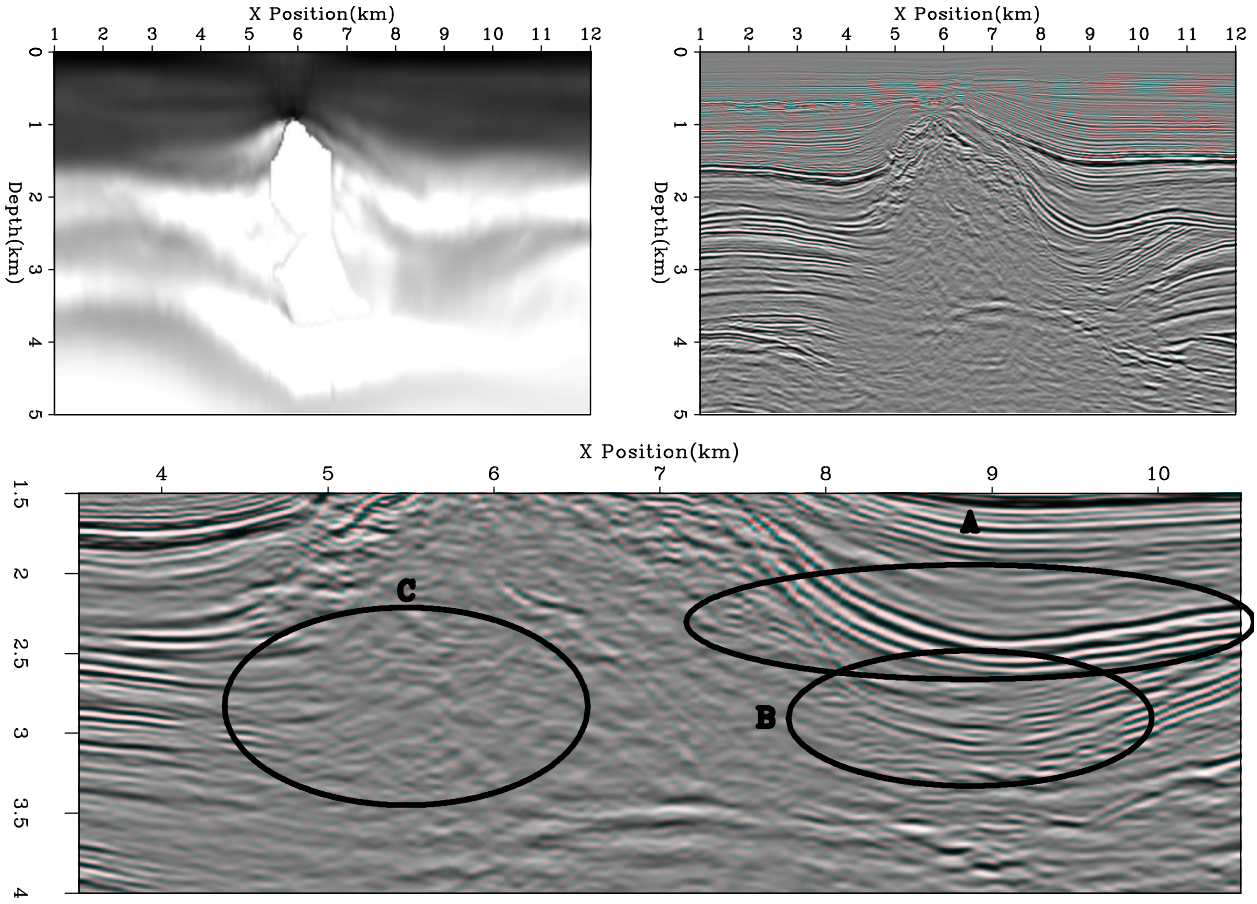

Figure 6: Data after one iteration using a constant ϵ. The top-left panel shows the velocity model and the top-right panel shows the migrated image using this velocity. The bottom panel shows a zoomed area around the salt body. Note the salt bottom,'A'; the valley structure at 'B'; and under the salt over-hang at 'C'. Note the improved image quality compared to Figure 4 and Figure 5. bob3-combo.vel1.eps [CR,M]

REFERENCES

Biondi, B., and Symes, W. W., 2002, Transformation to dip-dependent common image gathers: SEP–**112**, 65–82.

Claerbout, J., 1996, Conjugate-direction Huber regression: SEP–**92**, 229–235.

Claerbout, J. Geophysical Estimation by Example: Environmental soundings image enhancement:. http://sepwww.stanford.edu/sep/prof/, 1998.

Clapp, R. G., and Biondi, B., 1999, Preconditioning tau tomography with geologic constraints: SEP–**100**, 35–50.

Clapp, R. G., and Brown, M., 1999, Applying SEP's latest tricks to the multiple suppression problem: SEP–**102**, 91–100.

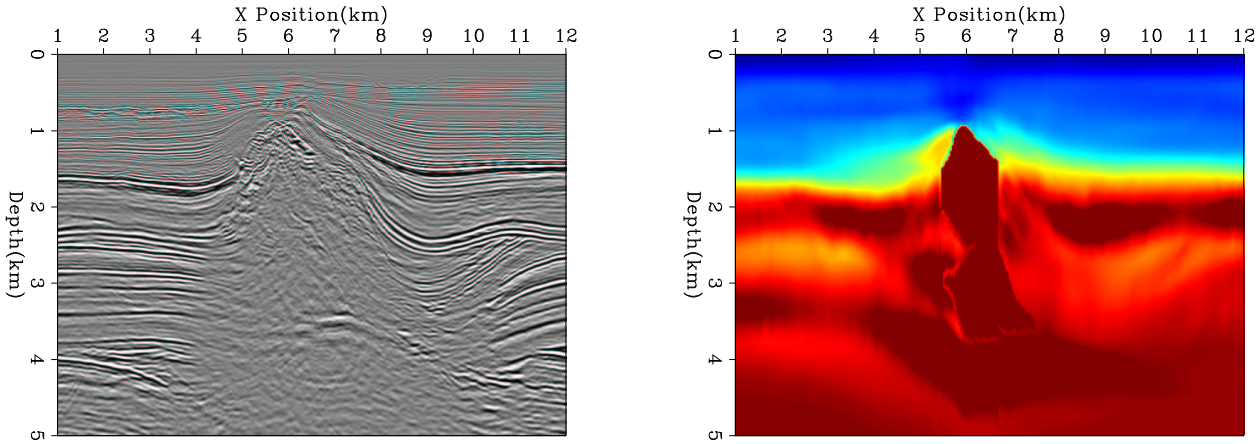

Figure 7: Data after one non-linear iteration using a reweighted least-squares. The top-left panel shows the velocity model and the top-right panel shows the migrated image using this velocity. The bottom panel shows a zoomed area around the salt body. Note the salt bottom,'A'; the valley structure at 'B'; and under the salt over-hang at 'C'. Note the improved image quality compared to Figure 4 and Figure 5. bob3-combo.vel1.steer [CR,M]

Clapp, R. G., Fomel, S., and Claerbout, J., 1997, Solution steering with space-variant filters: SEP–**95**, 27–42.

Clapp, R., 2001a, Ray-based tomography with limited picking: SEP–**110**, 103–112.

Clapp, R. G., 2001b, Geologically constrained migration velocity analysis: Ph.D. thesis, Stanford University.

Clapp, R. G., 2002, Ray based tomography using residual Stolt migration: SEP–**112**, 1–14.

Fomel, S., Clapp, R., and Claerbout, J., 1997, Missing data interpolation by recursive filter preconditioning: SEP–**95**, 15–25.

Guitton, A., 2000, Huber solver versus IRLS algorithm for quasi L1 inversion: SEP–**103**, 255–271.

Huber, P. J., 1973, Robust regression: Asymptotics, conjectures, and Monte Carlo: Ann. Statist., **1**, 799–821.

Kosloff, D., Sherwood, J., Koren, Z., MacHet, E., and Falkovitz, Y., 1996, Velocity and interface depth determination by tomography of depth migrated gathers: Geophysics, **61**, no. 5, 1511–1523.

Nichols, D., 1994, Velocity-stack inversion using $\mathbf{L_p}$ norms: SEP–**82**, 1–16.

Stork, C., 1992, Reflection tomography in the postmigrated domain: Geophysics, **57**, no. 5, 680–692.

van Trier, J., 1990, Tomographic determination of structural velocities from depth migrated seismic data: Ph.D. thesis, Stanford University.

Woodward, M. J., Farmer, P., Nichols, D., and Charles, S., 1998, Automated 3-D tomographic velocity analysis of residual moveout in prestack depth migrated common image point gathers:, *in* 68th Ann. Internat. Mtg Soc. of Expl. Geophys., 1218–1221.